HHS Public Access

Author manuscript

Inorganica Chim Acta. Author manuscript; available in PMC 2019 October 11.

Published in final edited form as:

Inorganica Chim Acta. 2019 September 1; 495: . doi:10.1016/j.ica.2019.118960.

Stabilizing a Ni^{II}-aqua complex via intramolecular hydrogen bonds: synthesis, structure, and redox properties

Deborah Brazzolotto, **Justin A. Bogart**, **Dolores L. Ross**, **Joseph W. Ziller**, **A. S. Borovik**

Department of Chemistry, University of California—Irvine, 1102 Natural Sciences II, Irvine, California 92697, United States.

Abstract

Hydrogen bonds within the secondary coordination sphere are effective in controlling the chemistry of synthetic metal complexes. Coupling the capacity of hydrogen bonds with those of redox-active ligands offers a promising approach to enhance the functional properties of transition metal complexes. These qualities were successfully illustrated with the $[NNN]^{3-}$pincer ligand *N,N*′-(azanediylbis(2,l-phenylene))bis(2,4,6-triisopropyl-benzene-sulfonamido ($[ibaps]^{3-}$) through the preparation of the Ni^{II}-OH2 complex, $[Ni^{II}(ibaps)(OH2)]^{-}$. The $[ibaps]^{3-}$ ligand contains two appended sulfonamido groups that support the formation of intramolecular hydrogen bonds. The bulky 2,4,6-triisopropylphenyl rings are necessary to ensure that only one ligand binds to a single metal ion. The molecular structure of the complex shows a square planar N3O primary coordination sphere and two intramolecular hydrogen bonds involving the aqua ligand. Electrochemical measurements in acetonitrile revealed two oxidation events at potentials below that of the ferrocenium/ferrocene couple. Oxidation with 1 equiv of ferrocenium produced the one-electron oxidized species, [Ni(ibaps)(OH2)]. Experimental and computational studies support this assignment.

Keywords

coordination chemistry; hydrogen bonds; redox-active ligands

Introduction

The designs of multidentate ligands are important in stabilizing specific metal oxidation states, promoting redox reactions in solution, and in tuning the reactivity of transition metal ions by influencing the steric and the electronic properties. Additionally, interest in ligands with radical character has increased following their use in the discovery of new types of reactivities.[1] Understanding the interactions between transition metal ions and non-innocent ligands has been crucial in order to design new catalysts.[2][3] Radical ligands are known to be found in several metalloenzymes such as the Fe-containing cytochrome P450s [4][5] as well as Cu-containing galactose oxidase.[6–8] These two classes of biological metal-radical species are formed differently and have distinct properties and stabilities, but share the common feature that the redox-activity of a coordinated ligand is essential for

Supporting Information contains Figure S1–S4 and Tables S1–S3. A summary of the crystallographic data is found in Table S4.

function.[2][9] Many synthetic redox-active ligand frameworks have been developed to improve the functional capabilities of metal complexes: significant improvements are found when these types of ligands are coordinated to 3*d* metal ions to promote multi-electron transformations.[2,3,10–15] Several reports have shown that redox properties of complexes with phenolate and porphyrin ligands can be further influenced by various factors including solvent, temperature, and the nature of the metal ion and substituents on the ligands. For instance, Ni^{II}-containing square planar complexes with phenolate ligands [16–18] can undergo a reversible one-electron oxidative process that was assigned to the Ni^{III}/Ni^{II} redox couple in coordinating solvent; however, the redox process changes to a phenolate-phenoxyl couple when done in non-coordinating solvents such as CH_2Cl_2.

Another design aspect of redox-active ligands is the incorporation of functional groups to control the secondary coordination sphere around the metal ion(s).[1,19–21] Examples include the pincer ligands of Gilbertson that contain appended amine groups that form intramolecular hydrogen bonds (H-bonds) with external ligands. We have recently introduced a new redox-active ligand ($[ibaps]^{3-}$) that contains a bis(aminophenyl)aminate ($[NNN]^{3-}$) framework and shows rich redox properties when coordinated to Fe and Ga ions.[14,15,21] This ligand also has the potential to control the secondary coordination sphere around the metal ion through the formation of H-bonds involving the two appended sulfonamido groups. In this report, we describe the preparation of $[Ni^{II}(ibaps)(OH2)]^{-}$ and its structural and redox properties. Our work demonstrates that $[ibaps]^{3-}$ can indeed support intramolecular H-bonds and undergo multi-electron oxidations.

Experimental

General Methods.

The preparations of metal complexes were completed under a dinitrogen atmosphere in a VAC drybox. Solvents were sparged with argon and dried over columns containing Q-5 and molecular sieves. All reagents were purchased from commercial suppliers and used as received unless otherwise noted. Potassium hydride as a 30% suspension in mineral oil was filtered and washed five times each with Et2O and pentane and dried under vacuum. Ferrocenium tetrafluoroborate ($FcBF_4$) was recrystallized before use. The ligand precursor *N*,*N*′-(azanediylbis(2,1-phenylene))bis(2,4,6-triisopropyl-benzene-sulfonamide, H_3ibaps) was prepared according to literature procedures.[21][22]

Physical Methods.

Electronic absorption spectra were recorded in a 5 mm cuvette on a Cary 60 UV-vis spectrometer. Negative-mode electrospray ionization mass spectra were collected using a Micromass MS Technologies LCT Premier mass spectrometer. Fourier transform infrared spectra were collected a Thermo Scientific Nicolet iS5 spectrophotometer with an iD5 Attenuated Total Reflectance (ATR) attachment in a dinitrogen filled glovebox. ^{1}H NMR spectra were recorded as $CDCl_3$ solutions on a Bruker CRYO500 or GN500 spectrometer and referenced to the residual solvent peak. Elemental analyses were performed on a Perkin-Elmer 2400 CHNS analyzer. Cyclic voltammetric experiments were conducted using a CHI600C electrochemical analyzer under an N_2 or Ar atmosphere with 0.1 M

tetrabutylammonium hexafluorophosphate as the supporting electrolyte. A 3.0-mm glassy carbon electrode was used as the working electrode with an AgCl reference electrode and a platinum wire counter electrode. Potentials are referenced to the $FeCp_2^+/FeCp_2$ redox couple.

X-ray Crystallographic Methods.

A Bruker SMART or Bruker Kappa APEX II CCD diffractometer was used to collect data. The APEX25 program package was used to determine the unit-cell parameters and for data collection. The raw frame data were processed using SAINT[23] and SADABS[24] to yield the reflection data file. Subsequent calculations were carried out using the SHELXTL[25] program. The analytical scattering factors[26] for neutral atoms were used throughout the analysis. Hydrogen atoms were included using a riding model.

Density Functional Theory.

All calculations were performed using gaussian 09 revision C.01 program.[27] For the geometry optimizations, the B3LYP functional with a 6–31g* basis set was used on all atoms. A CPCM solvent continuum model was used with acetonitrile as the solvent. Geometry optimization on the $[Ni(ibaps)(OH2)]^-$species was performed using the XRD coordinates as a starting point. The optimized geometry of $[Ni(ibaps)(OH2)]^-$was used initially for the geometry optimization on the [Ni(ibaps)(OH2)] species. Frequency calculations showed no negative frequencies indicating ground state geometries were obtained. TD-DFT calculations on the B3LYP optimized structures were performed using the CAM-B3LYP functional, which is reported to more accurately predict charge transfer transitions.[28] Molecular orbitals, spin density plots, and natural transition orbitals (NTOs) were rendered using the Chemcraft program.[29]

Preparative Methods. $(Et4N)[Ni^{II}(ibaps)OH_2]$.

A solution of H_3ibaps (0.20 g, 0.28 mmol) in 4 mL of dimethylacetamide (DMA) was treated with three equiv of solid KH (32 mg, 0.84 mmol). The reaction was stirred until gas evolution ceased and the solution was filtered. The $NiCl_2.6H_2O$ (67 mg, 0.28 mmol) salt was then added. After 1 h, Et_4NBr (59 mg, 0.28 mmol) was added to the reaction, which was stirred for an additional two hours before filtering the solution and removing the solvent under vacuum. The crude product was washed with 20 mL of Et_2O to remove DMA and volatiles were removed under reduced pressure. The resulting oil was dissolved in dichloromethane (DCM) and the product was crystallized from vapor diffusion of Et2O into a CH_2Cl_2 solution of the salt. The dark green needle crystals were washed with ether (3 × 10 mL) and filtered to remove KBr to obtain 101 mg (40% yield) of $(Et4N)[Ni^{II}(ibaps)OH2]$ as a green crystalline powder. ^1H NMR (500 MHz, CD_3CN): δ 1.11 (t, 12H), 1.22 (d, 36H), 2.86 (m, 8H), 3.16 (q, 6H), 6.4 (s, 4H), 6.88 (s, 4H), 7.16 (s, 4H). ESI-MS (5.10^{-5} M, CH_3CN, m/z,): Calcd. for $(Et4N)[Ni^{II}(ibaps)OH_2]$: 934.5; Found: 934.2, (positive ion mode). Elemental analysis calcd. For $C_{50}H_{76}N_4NiO_5S_2.\cdot 0.5CH_2Cl_2$ (978.45 g mol^{-1}): C, 61.99; H, 7.93; N, 5.73; Found for: C, 61.78; H, 8,36; N, 5.73. FTIR (ATAR, cm^{-1}, selected bands): 3230, 2956, 2927, 2867, 1600, 1570, 1556, 1491, 1480, 1451, 1438, 1418.

Results and Discussion.

Synthesis and Molecular Structure of $(Et_4N)[Ni^{II}(ibaps)(OH_2)]$.

The salt was prepared via 3-step synthesis (Scheme 1): H_3ibaps was allowed to react with three equiv of KH and the resultant mixture was treated with solid $NiCl_2{\cdot}6H_2O$ in one portion and stirred for 1 hour. Without isolation, the potassium salt was metathesized with tetraethylammonium bromide to afford $(Et_4N)[Ni^{II}(ibaps)(OH_2)]$, which was isolated in 40% yield as green crystals after recrystallization via slow diffusion of Et_2O into a solution of the tetraethylammonium salt. FTIR studies of the Ni^{II} complex, $[Ni^{II}(ibaps)(OH2)]^-$ contained a peak at 3230 cm^{-1} which is consistent with the υ(OH) of an aqua ligand. For example, the Ni^{II}-OH_2 complex with the tripodal sulfonamido ligand, *N*,*N*′, N″-[2,2′,2″-nitrilotris(ethane-2,l-diyl)]tris(2,4,6-trimethylbenzenesulfonamido, $[MST]^{3-}$) has a υ(OH) = 3259 cm^{-1}. [30] ^{1}′H NMR studies indicate that the complex is stable in solution with observable resonances associated with the $[ibaps]^{3-}$ ligand that are at different chemical shifts than that of the free ligand (Figure S1). Moreover, the chemical shifts of these signals suggest that $[Ni^{II}(ibaps)(OH_2)]^-$ is diamagnetic as expected for a Ni^{II} complex with a square planar ligand field.

The molecular structure of $(Et_4N)[Ni^{n}(ibaps)(OH_2)]$ was determined by X-ray diffraction methods and found that $[Ni^{II}(ibaps)(OH_2)]^-$ is indeed a mononuclear Ni^{II}-OH_2 complex in the crystalline phase (Figure 2, Tables 1 and S1). The Ni^{II} center resides in a slightly distorted square planar coordination geometry based on a $\tau_4 = 0.01$ in which an ideal square planar geometry has a $\tau_4 = 0$.[31] The primary coordination sphere contains a N_3O donor set composed of three deprotonated N-atoms from the $[ibaps]^{3-}$ ligand and a coordinated O-atom from an external water molecule. The Ni1-N1 bond length is 1.833(1) Å which is significantly shorter than the bond distances found for Ni1-N2 and Ni1-N3 which are 1.930(1) and 1.910(1) Å. A relatively short Ni1-N1 bond length of 1.835(2) Å was also found in the related Ni complex that contains an amido-bis(amine) pincer ligand. [32] The Ni1-O1 bond length is found to be 1.908(1) Å which is statistically shorter than the 2.074(2) Å bond length observed for the same bond in $[Ni^{II}MST(OH_2)]^-$−.[30] Note that the N1-Ni1-O1 and N2-N1-N3 bond angles are 176.02(6) and 169.09(6)°.

A distinguishing feature of $[Ni^{II}(ibaps)(OH_2)]^-$ is the presence of intramolecular H-bonds involving the coordinated aqua ligand. Both O-H bonds of the aqua ligand form H-bonds to the sulfonamido groups from $[ibaps]^{3-}$ as indicated by the O1···O2 and O1···O4 distances of 2.532(2) and 2.592(2) Å. In addition, HI and H2 were located from a difference-Fourier map and refined (x,y,z and U_{ISO}) to give O1-H1 and O1-H2 bond lengths of 0.84(3) and 0.83(3) Å and H1···O2 and H2···O4 distances of 1.75(3) and 1.86(3) Å. The presence of H-bonds causes the phenyl rings of the sulfonamido groups to be arranged in a *syn*-orientation on opposite faces of the $[ibaps]^{3-}$ ligand.

Redox Properties of $[Ni^{II}ibaps(OH_2)]^-$.

The electrochemical properties of $[Ni^{II}(ibaps)(OH_2)]^-$ were investigated using cyclic voltammetry in MeCN and showed two reversible one-electron oxidation events at $E_{1/2}$ (1) = −0.41 and $E_{1/2}$ (2) = −0.035 V (Figure 3). The redox performance changed when the

measurement was done in CH_2CL_2: the first oxidation process is reversible with an $E'_{1/2}$ = −0.59 V. The other redox event has an $E_{pa}{}'$ = −0.029 V but is not reversible. The loss of reversibility could be caused by interactions with Cl^- ions from the solvent (Figure 3). To check this possibility, various amounts of iPr_4NCl were added to the electrochemical cell containing $[Ni^{II}(ibaps)(OH_2)]^-$ in CH_3CN solution with 0.1 M $TBABF_6$ (Figure 4). The low-potential redox couple showed little change upon addition of the chloride ions and remained reversible. However, the second redox process becomes less reversible with increasing concentration of chloride ions, which supports the premise that this ion influences the second oxidation. Whether the chloride ion binds to the Ni center or displaces the aqua ligand are not known and requires further studies.

Oxidation and Related Spectral Changes.

The relatively low-potential associated with the first redox couple of $[Ni^{II}(ibaps)(OH_2)]^-$ and its reversibility under various conditions prompted us to investigate the product of this oxidation. The reaction was monitored spectrophotometrically in CH_3CN at room temperature (Figure 5). The absorbance spectrum of $[Ni^{II}(ibaps)(OH_2)]^-$ contained bands at λ_{max} = 770 nm (ε_M= 280) and λ_{max} = 470 nm (ε_M = 340) that are similar to features found for other N^{II}-OH_2 complexes[30] and are assigned to ligand-field transitions. These bands disappear when the complex is allowed to react with 1 equiv of $[Fe^{III}Cp_2]^+$ to produce $[Ni(ibaps)(OH_2)]$ (Scheme 1, Figure 5) that had more intense peaks at λ_{max} = 920 nm (ε_M = 4160), 790 (sh), 620 (ε_M = 1440), 458 nm (ε_M = 4320), and 360 nm (ε_M = 11600). These optical features are similar to those found in [Fe(ibaps)(bpy)] which has an electronic structure that did not allow assignment of formal oxidation state to the Fe center. The reaction was also probed using electron paramagnetic resonance (EPR) spectroscopy. The diamagnetic $[Ni^{II}(ibaps)(OH_2)]^-$ complex was EPR silent but after oxidation to $[Ni(ibaps)(OH_2)]$ a perpendicular-mode spectrum was observed with g-values at 2.28, 2.23 and 2.14. These signals are consistent with a rhombic species having an S = 1/2 spin ground state [33] but again, from these data we were unable to assign the unpaired spin to either a discrete ligand radical or a metal-centered oxidation.

Density Functional Theory.

We have used density functional theory to further examine the electronic structures of $[Ni^{II}(ibaps)(OH_2)]^-$ and $[Ni(ibaps)(H_2O)]$. In particularly, we wanted to probe if we could locate where the unpaired spin resided in $[Ni(ibaps)(H_2O)]$ that produced the EPR shown in Figure 6. Broken symmetry density functional theory (DFT) calculations were performed on $[Ni(ibaps)(OH_2)]^-$ (S = 0) and the one-electron oxidized $[Ni(ibaps)(H_2O)]$ (S = 1/2)species. A comparison between the calculated metal-ligand bond and H-bond distances (that is, O···O distances) for $[Ni^{II}(ibaps)(OH_2)]^-$ to those experimentally determined show a mean absolute deviation of 0.012 Å, which indicates excellent agreement between the calculations and experiment (Figure S2, Tables 1 and S1). It is noteworthy that the intramolecular H-bonds between the aqua ligand and the sulfonamido oxygen atoms were maintained in the ground-state optimized structure. The optimized structure for $[Ni(ibaps)(H_2O)]$ showed M-L bond distances of 1.852 Å, 1.949 Å, 1.939 Å, and 1.903 Å for Ni1-N1, Ni1-N2, Ni1-N3, and Ni1-O1 bonds, respectively (Figure 7A, Table S2). These bond distances indicated just a slight increase in M-N bond lengths of on average 0.017 Å and a small decrease in the M-O

bond length of 0.004 Å compared to the reduced species. Intramolecular H-bonds were also maintained with O1···O2 and O1···O4 distances of 2.57 Å and 2.62 Å, respectively, an average increase of 0.006 Å relative to the reduced species.

A relative Mulliken spin density analysis for [Ni(ibaps)(H_2O)] was used to qualitatively understand the degree of metal or ligand character for the first oxidation. This determination is indicated on the rendered spin density plots for [Ni(ibaps)(H_2O)] (Figure 7B). The four-coordinate [Ni(ibaps)(H_2O)] has significant spin density delocalized over the $[ibaps]^{3-}$ ligand and minimal spin density of 0.06 on the nickel which suggests the first oxidation is primarily ligand centered. Excited state TD-DFT calculations were also performed on $[Ni^{II}(ibaps)(OH_2)]$ to help assign the transitions in the electronic absorbance spectra. The calculated wavelengths of the vertical excitations are compared to the λ_{max} values of the experimentally observed transitions and show good agreement (Figure S3, Table S3). The nature of each transition as determined by the calculations is also indicated (Figures S4 and S5) and shows that those observed in the reduced $[Ni(ibaps)(H_2O)]^{-}$ complex were a result of d-d transitions while those in the oxidized [Ni(ibaps)(H_2O)] species were a result of MLCT transitions at lower energies and intraligand **π***-**π*** transitions at higher energies.

Summary

In this report we demonstrated that the trianionic pincer ligand $[ibaps]^{3-}$ can serve as a redox-active ligand and support H-bonds to an exogenous ligand. The molecular structure of $[Ni^{II}(ibaps)(OH_2)]^{-}$ revealed two intramolecular H-bonds are formed between a coordinated water molecule and the sulfonamido O-atoms of the $[ibaps]^{3-}$ ligand. Electrochemical measurements indicate that the complex has two oxidative redox events with both processes being reversible in acetonitrile. Oxidation of $[Ni^{II}(ibaps)(OH_2)]^{-}$ with 1 equiv of ferrocenium produced a species that is tentatively assigned as the one-electron oxidized complex, [Ni(ibaps)(OH_2)] which is paramagnetic and has an electronic absorbance spectrum with strong features throughout the visible region. Computational studies using DFT methods are in agreement with our experiments and suggest that the first oxidation predominately involves the $[ibaps]^{3-}$ ligand and that the intramolecular H-bonds still remain intact upon oxidation.

Supplementary Material

Refer to Web version on PubMed Central for supplementary material.

Acknowledgments

Acknowledgements are made to the National Institutes of Health, USA for financial support of this research (Grant GM050781).

References.

[1]. Derben LA, De Bruin Bc B, Heyduk AF, Non-innocent ligands, Chem. Commun 51 (2015) 1553–1554. www.rsc.org/chemcomm (accessed August 7, 2018).

[2]. Chirik PJ, Wieghardt K, Radical ligands confer nobility on base-metal catalysts, Science. 327 (2010) 794–795. doi:10.1126/science.H83281. [PubMed: 20150476]

[3]. Luca OR, Crabtree RH, Redox-active ligands in catalysis, Chem. Soc. Rev 42 (2013) 1440–1459. doi:10.1039/c2cs35228a. [PubMed: 22975722]

[4]. Rittle J, Green MT, Cytochrome P450 Compound I, Science. 330 (2010) 933–938. doi:10.1126/science.H93478. [PubMed: 21071661]

[5]. Yosca TH, Yosca TH, Rittle J, Krest CM, Onderko EL, Silakov A, Calixto JC, Behan RK, Green MT, Iron(IV)hydroxide pKa and the role of thiolate ligation in C-H bond activation by cytochrome P450, Science. 342 (2013) 825–829. doi:10.1126/science.l244373. [PubMed: 24233717]

[6]. Whittaker JW, The radical chemistry of galactose oxidase, Arch. Biochem. Biophys 433 (2005) 227–239. doi:10.1016/J.ABB.2004.08.034. [PubMed: 15581579]

[7]. Cowley RE, Cirera J, Qayyum Munzarin F., Rokhsana D, Hedman B, Hodgson KO, Dooley DM, Solomon EI, Structure of the reduced copper active site in preprocessed galactose oxidase: ligand tuning for One-Electron O2 activation in cofactor biogenesis, J. Am. Chem. Soc 138 (2016) 13219–13229. doi:10.1021/jacs.6b05792. [PubMed: 27626829]

[8]. Chaplin AK, Bernini C, Sinicropi A, Basosi R, Worrall JAR, Svistunenko DA, Tyrosine or tryptophan? Modifying a metalloradical catalytic site by removal of the Cys-Tyr cross-link in the galactose 6-oxidase homologue GlxA, Angew. Chem. Int. Ed 56 (2017) 6502–6506. doi:10.1002/anie.201701270.

[9]. Lecarme L, Chiang L, Moutet J, Leconte N, Philouze C, Jarjayes O, Storr T, Thomas F, The structure of a one-electron oxidized Mn(III)-bis(phenolate)dipyrrin radical complex and oxidation catalysis control via ligand-centered redox activity, Dalt. Trans 45 (2016) 16325–16334. doi:10.1039/c6dt02163h.

[10]. Crabtree Robert H., Multifunctional ligands in transition metal catalysis, New J. Chem 35 (2011) 18–23. doi:10.1039/c0nj00776e.

[11]. Dzik WI, Van Der Vlugt J. Ivar, Reek JNH, De Bruin B, Ligands that store and release electrons during catalysis, Angew. Chem. Int. Ed 50 (2011) 3356–3358. doi:10.1002/anie.201006778.

[12]. van der Vlugt JI, Cooperative catalysis with first-row late transition metals, Eur. J. Inorg. Chem (2012) 363–375. doi:10.1002/ejic.201100752.

[13]. Heyduk AF, Zarkesh RA, Nguyen AI, Designing catalysts for nitrene transfer using early transition metals and redox-active ligands, Inorg. Chem 50 (2011) 9849–9863. doi:10.1021/ic200911b. [PubMed: 21774482]

[14]. Nguyen AI, Blackmore KJ, Carter SM, Zarkesh RA, Heyduk AF, One-and two-electron reactivity of a tantalum(V) complex with a redox-active tris(amido) ligand, J. Am. Chem. Soc 131 (2009) 3307–3316. doi:10.1021/ja808542j. [PubMed: 19219982]

[15]. Nguyen AI, Zarkesh RA, Lacy DC, Thorson MK, Fleyduk AF, Catalytic nitrene transfer by a zirconium(IV) redox-active ligand complex, Chem. Sei 2 (2011) 166–169. doi:10.1039/c0sc00414f.

[16]. Thomas F, Ligand-centred oxidative chemistry in sterically hindered salen complexes: an interesting case with nickel, Dalt. Trans 45 (2016) 10866–10877. doi:10.1039/c6dt00942e.

[17]. Orio M, Jarjayes O, Kanso H, Philouze C, Neese F, Thomas F, Metal radical complexes X-Ray structures of copper(II) and nickel(II) radical Salen complexes: the preference of galactose oxidase for copper(II), Angew. Chem. Int. Ed 49 (2010) 4989–4992. doi:10.1002/anie.201001040.

[18]. Kochern A, Chiang L, Baptiste B, Philouze C, Leconte N, Jarjayes O, Storr T, Thomas F, Ligand-centered redox activity in cobalt(II) and nickel(II) bis(phenolate)-dipyrrin complexes, Chem. Eur. J 18 (2012) 14590–14593. doi:10.1002/chem.201202882. [PubMed: 23042520]

[19]. Borovik AS, Bioinspired Hydrogen Bond Motifs in Ligand Design: The Role of Noncovalent Interactions in Metal Ion Mediated Activation of Dioxygen, Acc. Chem. Res 38 (2005) 54–61. doi:10.1021/ar030160q. [PubMed: 15654737]

[20]. Cook SA, Borovik AS, Molecular designs for controlling the local environments around metal ions, Acc. Chem. Res 48 (2015) 2407–2414. doi:10.1021/acs.accounts.5b00212. [PubMed: 26181849]

[21]. Cook SA, Bogart JA, Levi N, Weitz AC, Moore C, Rheingold AL, Ziller JW, Hendrich MP, Borovik AS, Mononuclear complexes of a tridentate redox-active ligand with sulfonamido

groups: structure, properties, and reactivity, Chem. Sci 9 (2018) 6540–6547. doi:10.1039/c7sc05445a. [PubMed: 30310585]

[22]. Sharma SK, May PS, Jones MB, Lense S, Hardcastle KI, Macbeth CE, Catalytic dioxygen activation by Co(II) complexes employing a coordinatively versatile ligand scaffold, Chem. Commun 47 (2011) 1827–1829. doi:10.1039/c0cc04671j.

[23]. Bruker AXS Inc, SAINT Version8.34a. Madison, WI 2013, (n.d.).

[24]. Sheldrick GM, SADABS. Bruker AXS, Inc: Madison 2014, (n.d.).

[25]. Sheldrick GM, SHELXTL. Bruker AXS, Inc: Madison 2014, (n.d.).

[26]. Wilson AJC, Geist V, International tables for crystallography. Volume C: mathematical, physical and chemical tables. Kluwer academic publishers, Dordrecht/Boston/London 1992 (published for the International Union of Crystallography), 883 Seiten, ISBN 0-792-3-16-38X, Cryst. Res. Technol 28 (1993) 110–110. doi:10.1002/crat.2170280117.

[27]. Frisch MJ, Trucks GW, Schlegel HB, Scuseria GE, Robb MA, Cheeseman JR, Scalmani G, Barone V, Mennucci B, Petersson GA, Nakatsuji H, Caricato M, Li X, Hratchian HP, Izmaylov AF, Bloino J, Zheng G, Sonnenberg JL, Hada M, Ehara M, Toyota K, Fukuda R, Hasegawa J, Ishida M, Nakajima T, Honda Y, Kitao O, Nakai H, Vreven T, Montgomery JJA, Peralta JE, Ogliaro F, Bearpark M, Heyd JJ, Brothers E, Kudin KN, Staroverov VN, Keith T, Kobayashi R, Normand J, Raghavachari K, Rendell A, Burant JC, Iyengar SS, Tomasi J, Cossi M, Rega N, Millam JM, Kiene M, Knox JE, Cross JB, Bakken V, Adamo C, Jaramillo J, Gomperts R, Stratmann RE, Yazyev O, Austin AJ, Cammi R, Pomelli C, Ochterski JW, Martin RL, Morokuma K, Zakrzewski VG, Voth GA, Salvador P, Dannenberg JJ, Dapprich S, Daniels AD, Farkas O, Foresman JB, Ortiz JV, Cioslowski J, Fox DJ, Gaussian 09, Revision C.01, Gaussian, Inc., Wallingford CT (2010).

[28]. Peach MJG, Benfield P, Helgaker T, Tozer DJ, Excitation energies in density functional theory: an evaluation and a diagnostic test, J. Chem. Phys 128 (2008) 044118. doi:10.1063/1.2831900. [PubMed: 18247941]

[29]. Chemcraft, www.chemcraftprog.com, (n.d.).

[30]. Lau N, Sano Y, Ziller JW, Borovik AS, Terminal NiII-OH/-OH2 complexes in trigonal bipyramidal geometries derived from H2O, Polyhedron. 125 (2016) 179–185. doi:10.1016/j.poly.2016.11.015. [PubMed: 29170577]

[31]. Yang L, Powell DR, Houser RP, Structural variation in copper(I) complexes with pyridylmethylamide ligands: structural analysis with a new four-coordinate geometry index, $\tau 4$, Dalt. Trans (2007) 955–964. doi:10.1039/b617136b.

[32]. Csok Z, Vechorkin O, Harkins SB, Scopelliti R, Hu X, Nickel complexes of a pincer NN2 ligand: multiple carbon-chloride activation of CH2C12 and CHC13 leads to selective carbon-carbon bond formation, J. Am. Chem. Soc 130 (2008) 8156–8157. doi:10.1021/ja8025938. [PubMed: 18528995]

[33]. Jongbloed LS, Vogt N, Sandleben A, De Bruin B, Klein A, Van Der Vlugt J. Ivar, Nickel-alkyl complexes with a reactive PNC-pincer ligand, Eur. J. Inorg. Chem (2018) 2408–2418. doi:10.1002/ejic.201800168. [PubMed: 29937691]

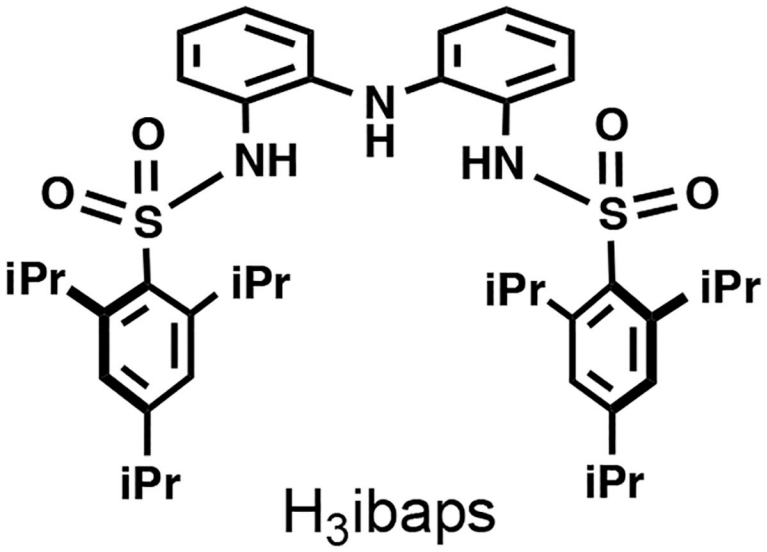

Figure 1.
The redox-active, H-bonding ligand H_3ibaps.

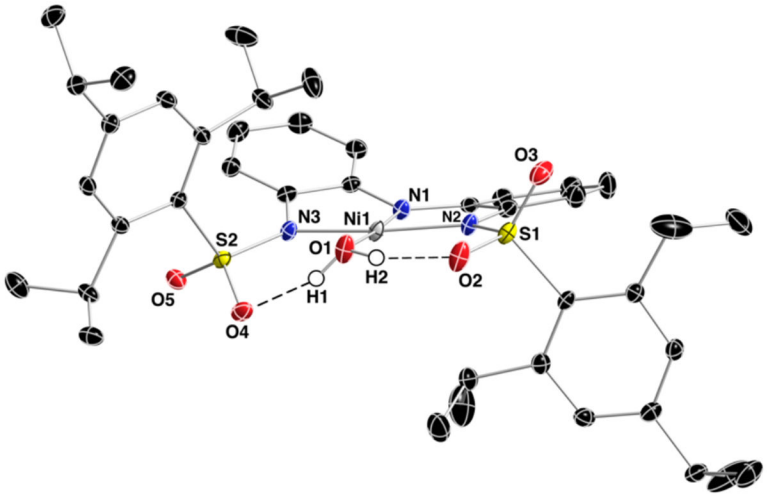

Figure 2.

Thermal ellipsoid diagram of $[Ni^{II}(ibaps)(OH_2)]^-$. The ellipsoids are drawn at 50% probability level and only the aqua hydrogen atoms are presented for clarity.

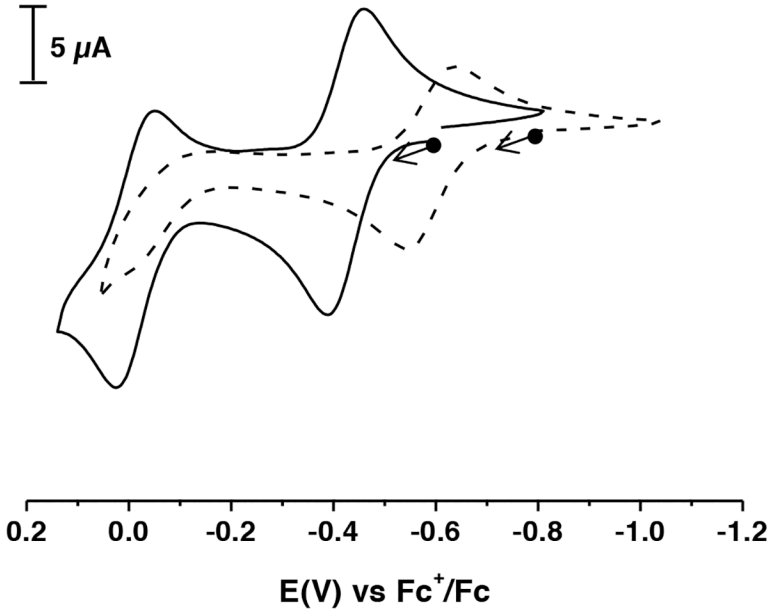

Figure 3.

Cyclic voltammograms of $[Ni^{II}(ibaps)(OH_2)]^{-}$ in MeCN (solid line) and in CH_2Cl_2 (dashed line) referenced to the $[Fe^{III/II}Cp2]^{+/0}$ couple. Conditions: 0.1 M of $TBAPF_6$, with a glassy carbon working electrode at 100 $mV{\cdot}s^{-1}$.

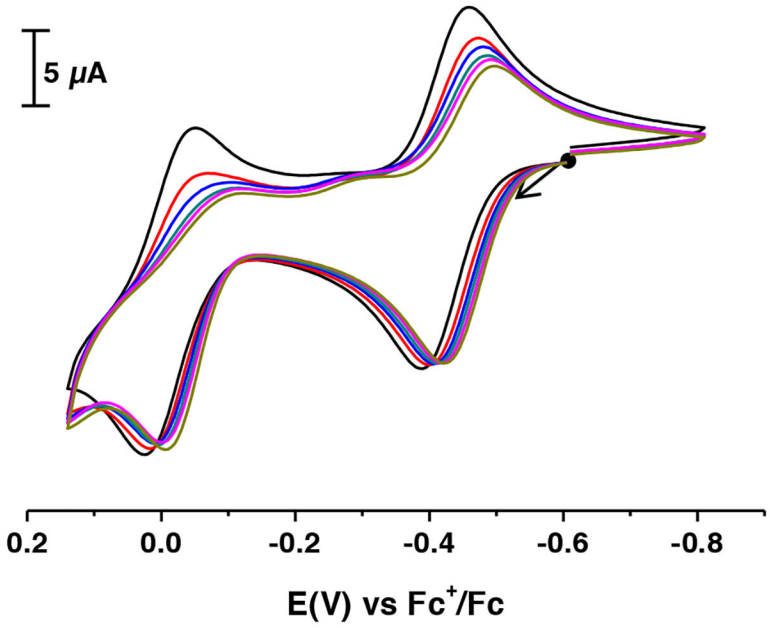

Figure 4.

Cyclic voltammograms of $[Ni^{II}(ibaps)(OH_2)]^-$ in MeCN after addition of 0 (black) 0.2 (red), 0.4 (blue), 0.6 (deep green), 0.8 (pink), 1 equiv. (green) of iPr_4NCl. 0.1M of $TBAPF_6$, on a glassy carbon electrode at 100 $mV.s^{-1}$. The CVs are referenced to the $[Fe^{III/II}Cp_2]^{+/0}$ couple.

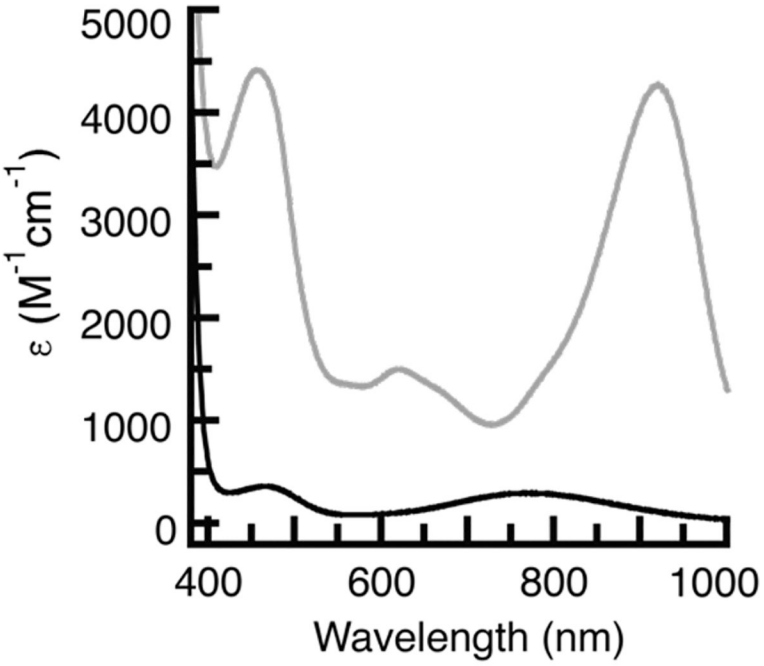

Figure 5.

Electronic absorbance spectra of $[Ni^{II}(ibaps)(OH_2)]^-$ (—) and after addition of 1 eq of $[Fe^{III}Cp_2]BF_4$ (—). Spectra were recorded at room temperature in CH_3CN. Concentrations for $[Ni^{II}(ibaps)(OH_2)]^-$: 1.0 mM and for generation of $[Ni(ibaps)(OH_2)]$: 0.25mM.

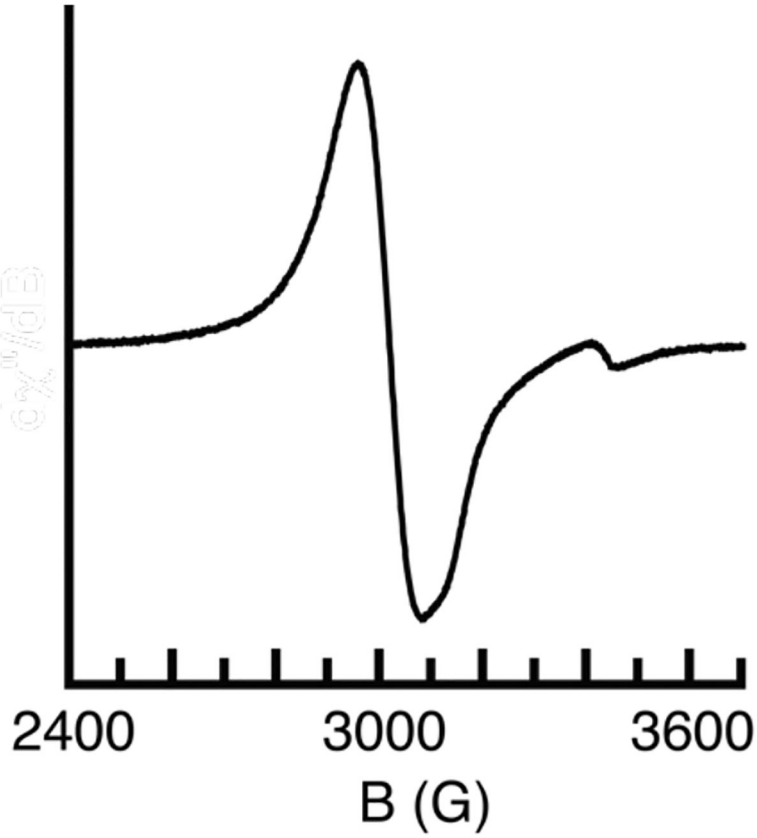

Figure 6.

EPR spectrum of [Ni^{II}(ibaps)(OH_2)]-after addition of 1 eq of [$Fe^{III}Cp_2$]BF_4. Spectrum was recorded at X-band as a frozen CH_3CN solution at 10 K.

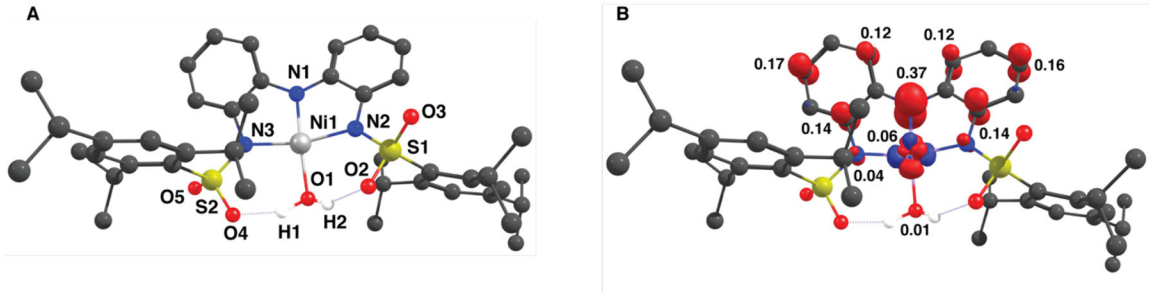

Figure 7.

DFT computed structure **(A)** and rendered spin density plot **(B)** for [Ni(ibaps)(H_2O)].

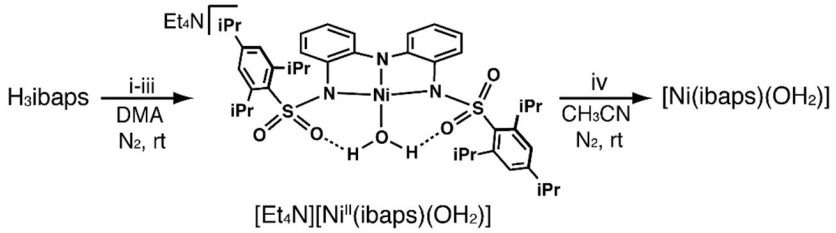

Conditions: i, 3 KH, -3 H_2; ii, $NiCl_2 \cdot 6H_2O$, -2 KCl; iii, Et_4NBr, -KBr; iv, $[Fe^{III}Cp_2]BF_4$, $-Et_4NBF_4$

Scheme 1.

Table 1.

Selected structural parameters for of [Ni(ibaps)(H_2O)]$^-$ and a comparison to those calculated from DFT.

Metric	Exp (Å or °)	Calc (Å or °)	|Δ|
Ni1-N1	1.833(1)	1.833	0.001
Ni1-N2	1.929(1)	1.936	0.007
Ni1-N3	1.910(1)	1.921	0.011
Ni1-O1	1.908(1)	1.907	0.002
O1-H1	0.84(3)	0.99	0.15
O1-H2	0.83(3)	0.99	0.16
O1···O2	2.532(2)	2.566	0.033
O1···O4	2.592(2)	2.611	0.019
H1···O2	1.75(3)	1.62	0.13
H2···O4	1.86(3)	1.69	0.17
N1-Ni1-O1	176.02(6)	170.51	5.51
N1-Ni1-N3	84.11(6)	84.33	0.22
O1-Ni1-N3	93.05(6)	94.82	1.77
N1-Ni1-N2	85.06(6)	84.78	0.28
O1-Ni1-N2	97.70(6)	96.92	0.78
N3-Ni1-N2	169.09(6)	167.56	1.53
O1-H1-O2	155(3)	158	3
O1-H2-O4	147(3)	152	5